A blue to green tunable $Ba_3GdP_3O_{12}$:Tb^{3+} nanophosphor: structural and opto-electronic analysis

Heena Dahiya[1] · Mandeep Dalal[2] · Anju Siwach[1] · Manju Dahiya[1] · V. B. Taxak[2] · S. P. Khatkar[2] · Dinesh Kumar[1]

Abstract

A series of blue–green $Ba_3Gd_{(1-x)}P_3O_{12}$: xTb^{3+} nanocrystals has been successfully prepared via the urea-assisted solution-combustion method. Its structure, morphology, energy-transfer mechanism, photoluminescent (PL) excitation-emission and decay time behavior were investigated in detail employing powder X-ray diffraction (XRD), Transmission Electron Microscopy (TEM), Diffuse Reflectance (DR) and PL spectroscopy. The Rietveld analysis exposed the cubic phase of all the nanophosphors with I-43d (220) space group and infers that Gd^{3+} ions can be well substituted by Tb^{3+} ions without any major alteration in the crystal prototype of the host lattice. The optical band-gap of the host was calculated to be 4.9 eV, unveiling the high potential as a host for lanthanide activators. Under the excitation at $\lambda_{ex} = 224$ nm, the photoluminescent emission spectra exhibited the two main characteristic peaks at 545 nm and 487 nm as a result of $^5D_4 \rightarrow {}^7F_5$ (green and magnetic-dipole) and $^5D_4 \rightarrow {}^7F_6$ (blue and electric-dipole) transitions, respectively. The decay analysis showed that the activator occupies a single crystallographic site, a fact that is also supported by the Rietveld refinement. The critical distance of the energy transfer (19.87 Å) integrated with Dexter's modeling inferred about the energy migration (dipole–dipole). The PL result showed that the blue-to-green tunable emission can be achieved simply via varying the dopant concentration, with 7 mol% as the optimum concentration for standard CIE coordinates of green emission. All the results suggest that $Ba_3Gd_{(1-x)}P_3O_{12}$: xTb^{3+} crystals may find their use as a green phosphor component in display devices and solid-state lighting.

1 Introduction

In the recent years, scientists all around the world have been making efforts in producing nanophosphor materials as these are considered as very valuable asset in the field of optical applications such as solid-state laser devices, optical amplifiers, light emitting diodes (LED's), solar cells, X-ray medical radiography, cathode ray-tubes, sensor technology, optical markers, and plasma display panels [1–4]. The motive is to design and develop a near-ultraviolet (NUV) excited but eco-friendly phosphor material with better luminescence, long emission lifetime, high thermal stability, narrow emissions bands and with reasonable product reliability [5–9]. In this context, rare-earth trivalent ions play an important role when

incorporated in a suitable host matrix; which is obviously due to their outstanding luminescent properties, arising from the intra-configurational $4f$–$4f$ and $4f$–$5d$ transitions [10]. Furthermore, it is a quite well-known fact that Tb^{3+} ions can act as activators for green-emitting nanophosphor in various suitable host matrixes. Many researchers are paying attention to grow the Tb^{3+}-based green-emitting phosphor crystals. The reason being for the high popularity of Tb^{3+} ions as an activator is a dominant peak at around 545 nm ($^5D_0 \rightarrow {}^7F_5$ transition) which can be tweaked to a great extent due to the large electric-dipole character [11–14]. Nonetheless, other transitions originating from the ^5D_J excited state are also of great significance as far as visible emission is concerned.

Though there are some reports on the single Tb^{3+}-doped $Ba_3GdP_3O_{12}$ compositions via conventional solid-state method [15, 16]; however, to the best of the author knowledge, concentration-dependent PL properties, Rietveld analysis and synthesis via other chemical routes are unavailable to date. This paper covers the fabrication of a series of $Ba_3Gd_{(1-x)}P_3O_{12}$: xTb^{3+} ($x = 0.02, 0.03, 0.04, 0.05, 0.06, 0.07, 0.08$) via urea-based solution combustion method for the first time. The structural prototype, phase purity, surface

✉ Dinesh Kumar
    dineshdalal8@rediff.com

[1] Department of Chemistry, Deenbandhu Chhotu Ram University of Science & Technology, Murthal, Sonepat 131039, India

[2] Department of Chemistry, Maharshi Dayanand University, Rohtak 124001, India

morphology, emission dynamics and optical properties of the synthesized nanophosphor were characterized by X-ray diffraction technique, Rietveld refinement using FULLPROF program, transmission electron microscopy, decay time and photoluminescence spectroscopy, respectively. The corresponding critical distance (R_c) for energy transfer was determined experimentally and then employed to demonstrate the mechanism responsible for the concentration quenching arising from energy-migration among the neighboring Tb^{3+} ions. The assessed outcomes display that the solution-combustion approach for the synthesis of a blue–green tunable nanophosphor provided a fast and economic technique which diminished the sintering temperature as well as the duration of the heat treatment. The synthesized phosphor samples were found with high purity, single-phased crystalline nanostructure, better luminescent intensity than the sample prepared from the solid-state method. So, the obtained nanophosphors can be utilized as a solid-state lighting nanomaterial.

2 Experimental setup

2.1 Material and synthesis

A series of $Ba_3Gd_{(1-x)}Tb_xP_3O_{12}$ ($x = 0.02$, 0.03, 0.04, 0.05, 0.06, 0.07, 0.08) nanophosphors was prepared from urea-assisted solution combustion technique. The initial materials used were $Gd(NO_3)_3 \cdot 6H_2O$, $Tb(NO_3)_3 \cdot 5H_2O$, $Ba(NO_3)_2$, $(NH_4)_2HPO_4$ and NH_2CONH_2 were of analytical grade. In a typical procedure, all the nitrates in stoichiometric quantities were dissolved in a minimal amount of deionized water. The quantity of urea used as a fuel for the propellant reaction was calculated by using total oxidizing and reducing valencies of oxidizer and fuel [17]. After obtaining the homogenous solution, the final solution was placed in a preheated furnace kept at 500 °C for 15–20 min. Initially, the solution boils with the liberation of huge amounts of gases. These gases burnt and ignited with a blaze yielding a foamy solid. Further, the obtained voluminous sample was effortlessly milled to get fine precursor powder by using an agate mortar and annealed at 1200 °C for 5 h in the air to attain better crystallinity.

2.2 Materials characterization

Powder X-ray diffraction (PXRD) patterns of all the samples were evaluated by a Rigaku make (Ultima-IV) powder X-ray diffractometer from $2\theta = 10°–80°$ at a scanning rate of 2°/min using Cu Kα as radiation source, while the tube voltage and tube current were kept constant at 40 kV and 40 mA, correspondingly. Furthermore, the phase analysis and refinement of parameters of the synthesized nanophosphor

sample was achieved with the Rietveld method in FULLPROF software package. The isotropic displacement and fractional coordinates of all the mixed atoms were constrained during the refinement. Technai-G^2 transmission electron microscope (TEM) was used to study the surface morphology and crystallite size. The Diffuse Reflectance Spectrum (DRS) of all the powder samples were recorded in the wavelength ranging from 200 to 800 nm using Shimadzu UV-3600 accessorized with an integrated sphere and $BaSO_4$ as reference standard was used. Edinburgh fluorescence spectrophotometer (FLS-980) equipped with 450 W Xenon lamp as the excitation source was used to study the photoluminescence spectra, color coordinates and decay curves of terbium doped $Ba_3GdP_3O_{12}$ nanophosphors. The photo-multiplier tube (PMT) voltage was set at 400 V while the excitation-emission bandwidths were fixed at 2.5 nm. The whole process was performed at room temperature and atmospheric pressure.

3 Result and discussion

3.1 Structural analysis

The analysis of the crystal structure and corresponding phase purity for all the samples was performed by powder X-ray diffraction (PXRD) technique. Figure 1 displays the XRD patterns of the complete $Ba_3Gd_{(1-x)}Tb_xP_3O_{12}$ ($x = 0.02$, 0.03, 0.04, 0.05, 0.06, 0.07, 0.08) nanophosphor series along with the standard JCPDS card No. 29-0163. It can be seen that all the peaks of the XRD patterns are well-matched with the standard data. The cubic phase with a space group of I-43d without any other impurity peak indicates that Tb^{3+} ions substitute the Gd^{3+} ions without disturbing the crystal structure
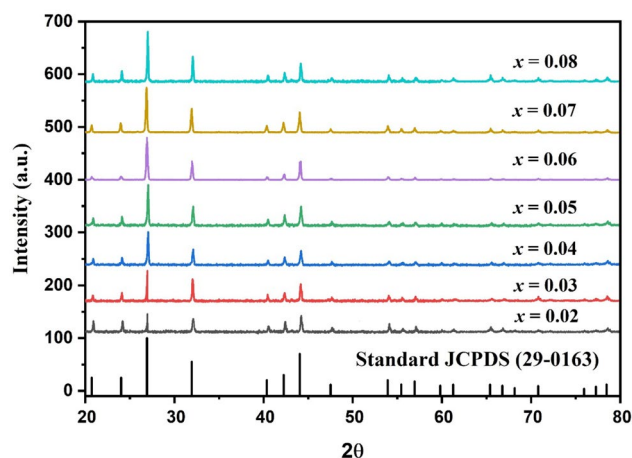

Fig. 1 XRD profile of $Ba_3Gd_{1-x}Tb_xP_3O_{12}$ ($x = 0.02–0.08$) nanophosphors along with standard JCPDS data of $Ba_3GdP_3O_{12}$ (Color figure online)
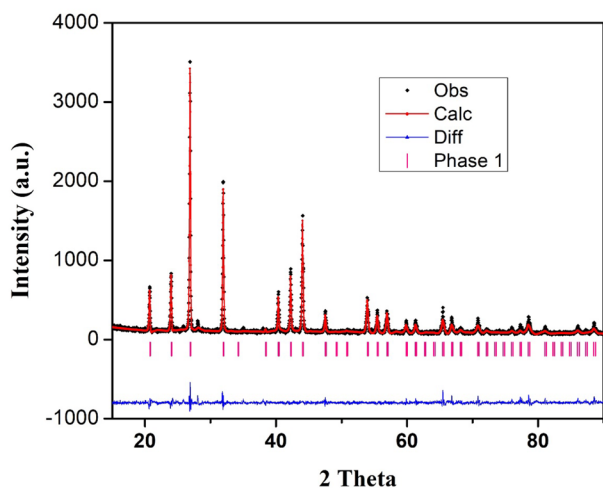
Fig. 2 Rietveld refinement of $Ba_3Gd_{0.93}Tb_{0.07}P_3O_{12}$ nanocrystals, $\chi^2 = 1.94$, $R_p = 9.03(\%)$, $R_{wp} = 11.7(\%)$ and $R_{exp} = 8.43(\%)$ (Color figure online)

Table 1 Comparison of crystal structure data of $Ba_3Gd_{0.93}Tb_{0.07}P_3O_{12}$ nanophosphors with standard $Ba_3GdP_3O_{12}$

Formula	$Ba_3GdP_3O_{12}$	$Ba_3Gd_{0.93}Tb_{0.07}P_3O_{12}$
Formula weight	854.15	854.27
Symmetry	Cubic	Cubic
Space group	I-43d (220)	I-43d (220)
$a = b = c$ (Å)	10.4780	10.4737
$\alpha = \beta = \gamma$ (°)	90	90
Volume (Å³)	1150.36(16)	1148.95(15)
Z	4	4
Density (g/cm³)	4.9284	4.9371
Pearson code	tI76	tI76
Wyckoff sequence	i2h5ba	i2h5ba

prototype. In support of the above-mentioned statement, Rietveld refinement in FULLPROF software was achieved for $Ba_3Gd_{0.93}Tb_{0.07}P_3O_{12}$ nanocrystal using its PXRD profile. Figure 2 displays the calculated (red line) and observed (black line) patterns; the deviation of experimental and theoretical data (blue); and the corresponding Bragg positions (pink). The

refinement converged to a reasonable fit with $R_p = 9.03(\%)$, $R_{wp} = 11.7(\%)$, $R_{exp} = 8.43(\%)$ and $\chi^2 = 1.94$. The refinement process yielded various structural parameters such as $a = b = c = 10.445$ Å, $V = 1111$ Å³ and $Z = 4$. Table 1 shows the comparative study of the crystal structure data of the host and of $Ba_3Gd_{0.93}Tb_{0.07}P_3O_{12}$ system. The comparison clarifies that there is a slight decrease in the unit cell volume from 1151.009 to 1148.95 Å³ upon substitution of Gd^{3+} ions by Tb^{3+} ions, which can be explained on the account of smaller ionic radius of Tb^{3+} (92.3 pm) than Gd^{3+} (93.8 pm), and hence decreases the density of the doped nanophosphor [18]. The refined atomic positions and their occupancies are tabularized in Table 2; whilst Table 3 displays the several interatomic distances (Å) in $Ba_3Gd_{0.93}Tb_{0.07}P_3O_{12}$ nanocrystal.

Moreover, the average crystallite size was evaluated by using the full-width at half-maxima (FWHM) of the most prominent diffraction peak for $Ba_3Gd_{0.93}Tb_{0.07}P_3O_{12}$ nanophosphor from Scherrer's equation [19, 20]:

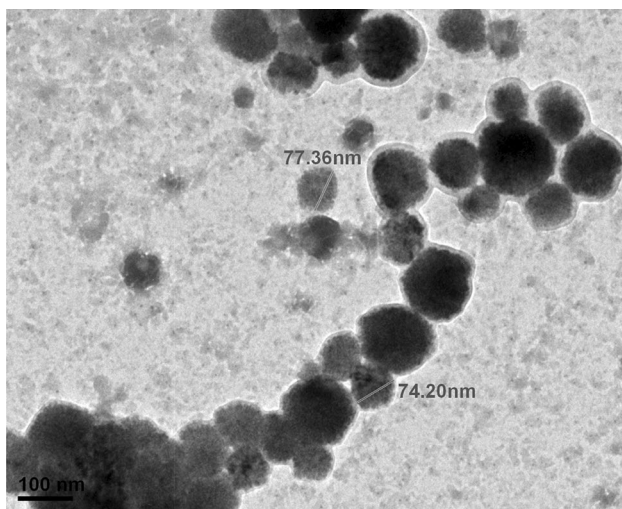$$D = \frac{0.941\lambda}{\left(B_O^2(2\theta) - B_{Si}^2(2\theta)\right)^{\frac{1}{2}}Cos(\theta)} \tag{1}$$

where D is the average crystallite size, λ the X-ray wavelength (0.15406 nm), θ is the diffraction angle; $\beta_{Si}(2\theta)$ and $\beta_0(2\theta)$ are the full-width at half-maximum (FWHM, in radian) of the standard silicon and of the synthesized sample, correspondingly. The results of the particle size suggested a range of 40–70 nm. Additionally, to study the surface morphology along with particle size of as-prepared $Ba_3Gd_{1-x}Tb_xP_3O_{12}$ nanophosphor samples Transmission Electron Microscopy (TEM) was carried out. Figure 3 displays the TEM micrograph of the $Ba_3Gd_{0.93}Tb_{0.07}P_3O_{12}$ nanophosphor, showing well-dispersed particles with minute agglomeration magnified at 100 nm. Therefore, it is quite safe to say that the results from Scherrer's equation and TEM micrography, are found to be in good agreement with each other. Later on, the Strain (ε) and Dislocation density (δ) were calculated for all the synthesized nanophosphors and are reported in Table 4 utilizing the following equations [21, 22]:

$$\varepsilon = \frac{\beta Cos\theta}{4} \tag{2}$$

Table 2 Refined positions of all atoms and occupancy data for the $Ba_3Gd_{0.93}Tb_{0.07}P_3O_{12}$ nanocrystals

Atom label	Ion type	Wyckoff positions	Site	Fill	x/a	y/b	z/c	U (Å²)
Ba	Ba^{2+}	16c	0.3	0.74901	0.0641(2)	0.0641(2)	0.0641(2)	0.0443
Gd	Gd^{3+}	16c	0.3	0.2509	0.0641(2)	0.0641(2)	0.0641(2)	0.0443
Tb	Tb^{3+}	16c	0.3	0.0037	0.0641(2)	0.0641(2)	0.0641(2)	0.0443
P	P^{5+}	12a	−4	1.3389	3/8	0	1/4	0.0377
O1	O^{2-}	48e	1	0.7121	0.576 (5)	0.356 (6)	0.680 (8)	0.0771
O2	O^{2-}	48e	1	0.2879	0.524 (5)	0.341 (5)	0.695 (5)	0.0448

Table 3 Interatomic distance (Å) of all designated cations of the particular $Ba_3Gd_{0.93}Tb_{0.07}P_3O_{12}$ nanophosphor

Bond type	Distance	Bond type	Distance
Ba/Gd/Tb–O1	2.4977 × 3	O1–O1	2.7322 × 1
Ba/Gd/Tb–O2	2.7415 × 3	O1–Ba/Gd/Tb	2.8109 × 1
Ba/Gd/Tb–O2	2.7443 × 3	O1–O2	2.9827 × 1
Ba/Gd/Tb–O1	2.8109 × 3	O1–Ba/Gd/Tb	2.8109 × 1
P–O2	1.2284 × 3	O2–O1	0.5884 × 1
P–O2	1.2286 × 1	O2–P	1.2284 × 1
P–O1	1.4826 × 3	O2–O1	1.8954 × 1
P–O1	1.4827 × 1	O2–O2	1.9713 × 1
O1–O2	0.5882 × 1	O2–O2	2.0232 × 2
O1–P	1.4825 × 1	O2–O1	2.3193 × 1
O1–O2	1.8954 × 1	O2–O1	2.3476 × 1
O1–O1	2.2493 × 2	O2–Ba/Gd/Tb	2.7416 × 1
O1–O2	2.3193 × 1	O2–Ba/Gd/Tb	2.7444 × 1
O1–O2	2.3475 × 1	O2–O1	2.9827 × 1
O1–Ba/Gd/Tb	2.4977 × 1		

Table 4 The strain and dislocation density parameters in $Ba_3Gd_xTb_{(1-x)}P_3O_{12}$ nanophosphor series

Tb^{3+} concentrations (mol%)	Strain × 10^{-3}	Dislocation density (δ) (10^4 × nm^{-2})
2	0.011	0.486
3	0.011	0.491
4	0.012	0.612
5	0.013	0.713
6	0.015	0.997
7	0.017	1.163
8	0.017	1.189

Fig. 3 TEM micrographs of $Ba_3Gd_{0.93}Tb_{0.07}P_3O_{12}$ powder calcined at 1100 °C

Fig. 4 The relationship between the absorption coefficient and photon energy for $Ba_3GdP_3O_{12}$ host matrix and (inset) corresponding diffuse reflectance spectra
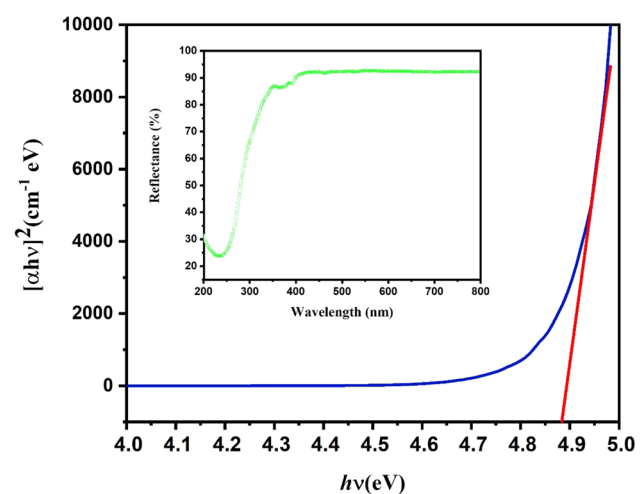
$$\delta = \frac{1}{D^2} \quad (3)$$

Furthermore, the variance of the absorption coefficient against photon energy, along with the reliable diffuse reflectance spectra (inset), for the $Ba_3GdP_3O_{12}$ host is shown in Fig. 4. The Kubelka–Munk function is utilized to evaluate the magnitude of the optical band gap (E_g) for solids. So, the values of various kinds of band-gap can be implicated by using the below relation [23]:

$$\left[F(R_\infty h\nu)\right]^n = C(h\nu - E_g) \quad (4)$$

where C is a proportionality constant, $h\nu$ denotes the energy of the photon and E_g signifies the band gap (eV). The symbol n is 0.5, 2, 1.5 and 3 for allowed indirect, allowed direct, forbidden direct and forbidden indirect transitions, respectively. $F(R_\infty)$ implies the Kubelka–Munk function whose standards is well-defined as [24]:

$$F(R_\infty) = \frac{(1 - R_\infty)^2}{2R_\infty} = \frac{K}{S} \quad (5)$$

where K and S are the absorption and scattering coefficients, correspondingly; while R_∞ represents the ratio of R_{sample} to $R_{standard}$. The extrapolation of the line with $F(R_\infty) h\nu = 0$ exposed a band-gap of 4.88 eV.

3.2 Optical properties

Figure 5 displays the photoluminescence excitation (PLE) spectrum of Tb^{3+} ions doped $Ba_3GdP_3O_{12}$ nanophosphor obtained when monitored at λ_{em} of 545 nm due to ($^5D_4 \rightarrow {^7F_5}$) transition. The PLE revealed that the spectrum consists of a broad band ranging from 200 to 240 nm (centered at 224 nm), which obviously arises due to the transition from ground state $4f^8$ to the excited state $4f^7\,5d^1$ (f–d inter-configurational transition) in trivalent terbium ions [25, 26]. Along with this, weak absorptions at 273 nm and 311 nm are also found and are assigned as the intra-configurational 4f–4f transitions of the Tb^{3+} ions in $Ba_3GdP_3O_{12}$ host. Among these peaks, the broad-band at 224 nm has been chosen to evaluate the emission spectra of $Ba_3GdP_3O_{12}$:Tb^{3+} (2–8 mol%).

The photoluminescence emission spectrum of Tb^{3+} doped nanophosphors mainly consists of several prominent peaks in the wavelength region of 500–700 nm. The PL emission spectra shows the peaks at 415 nm, 436 nm and 456 nm are arising from $^5D_3 \rightarrow {^7F_J}$ (J = 5, 4, 3) transitions, whereas the transitions at 487 nm, 545 nm, 582 nm and 620 nm appear from $^5D_4 \rightarrow {^7F_J}$ (J = 6, 5, 4, 3), respectively [27–30]. Among these peaks, transitions from $^5D_3$ are responsible for the blue color of the nanophosphors while transitions from the $^5D_4$ state are responsible for the characteristic green emission in the case of trivalent terbium ions. It can be seen from Fig. 6, that the most intense peak located at 545 nm ($^5D_4 \rightarrow {^7F_5}$) will be primarily responsible for the emission color of the nanophosphors. Furthermore, the PL emission intensity of the peaks from the $^5D_4$ excited state shows remarkable enhancement on increase in activator concentration in the host matrix up to 7 mol% but decreases afterward as shown in Fig. 7. This decrease in the PL intensity for $^5D_4 \rightarrow {^7F_J}$ transitions can be ascribed to the concentration quenching effect. The reason for the concentration quenching in PL spectra can be explained on the basis of decreasing distance
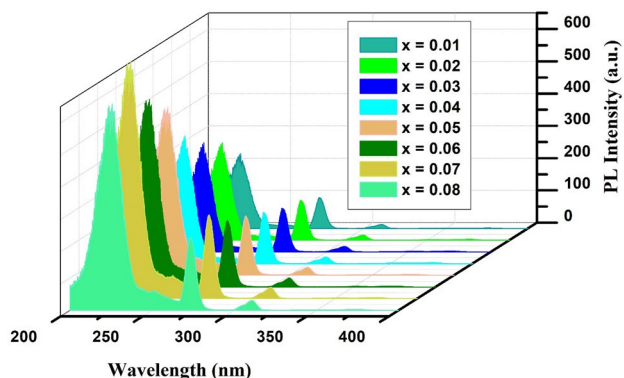

Fig. 6 Emission spectra of $Ba_3Gd_{1-x}Tb_xP_3O_{12}$ (x = 0.02–0.08) nanophosphor excited at λ_{ex} = 224 nm (Color figure online)

between the neighboring Tb^{3+} ions in the host matrix, resulting in a considerable increase in the energy transfer via non-radiative process [31, 32].

Besides this, it is also worthy to note that the intensity of the emission peaks arising from $^5D_3 \rightarrow {^7F_J}$ transitions decreases with the increase in the Tb^{3+} ions concentration as shown in Fig. 8. This leads to the shift in the emission color from light blue to light green. The energy level plot for the Tb^{3+}-doped $Ba_3GdP_3O_{12}$ also includes the DC (down-conversion) energy transfer mechanism through radiative as well as non-radiative paths. Upon excitation, the Tb^{3+} ions get excited from the $^7F_6$ ground state to higher energy state (224 nm); which in turn gets depopulated non-radiatively to enrich the lower energy levels ($^5D_3$, $^5D_4$) of Tb^{3+} ions. The tunability of the emission color for terbium ions may be attributed to the cross-relaxation phenomenon. The same
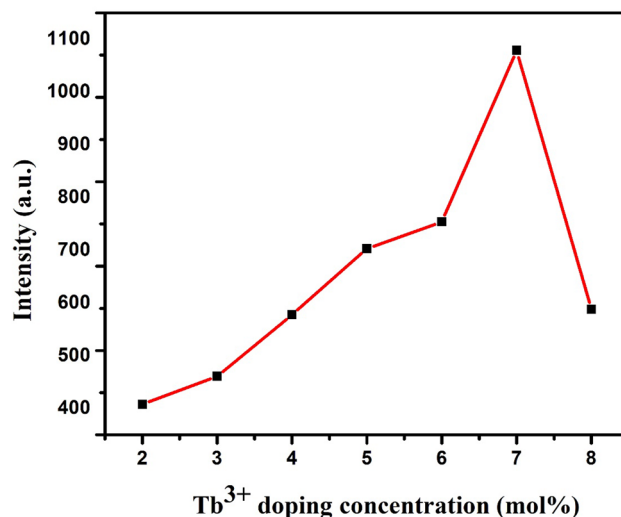

Fig. 5 Excitation spectra of $Ba_3Gd_{1-x}Tb_xP_3O_{12}$ (x = 0.01–0.08) nanophosphor studied at λ_{em} = 545 nm (Color figure online)

Fig. 7 Variation of emission intensity for $Ba_3Gd_{1-x}Tb_xP_3O_{12}$ nanophosphors (x = 0.02–0.08) at 545 nm as a function of Tb^{3+} concentration, sintered at 1200 °C

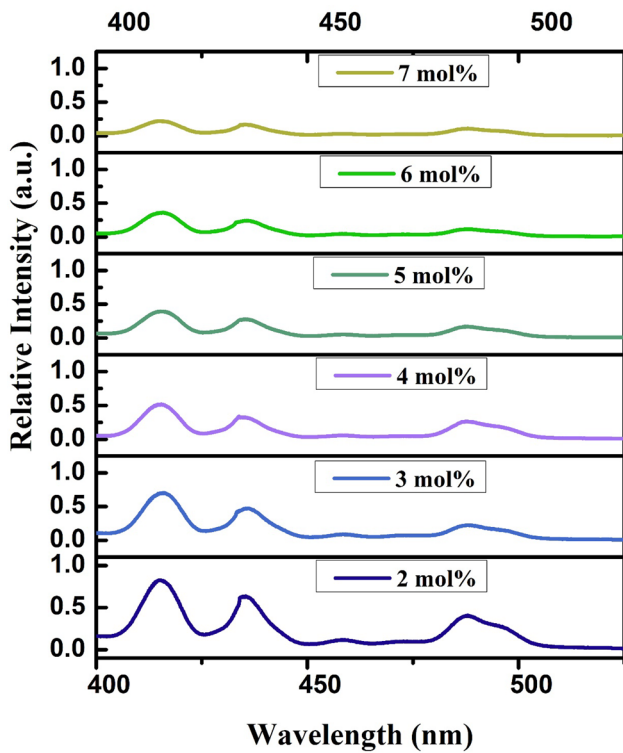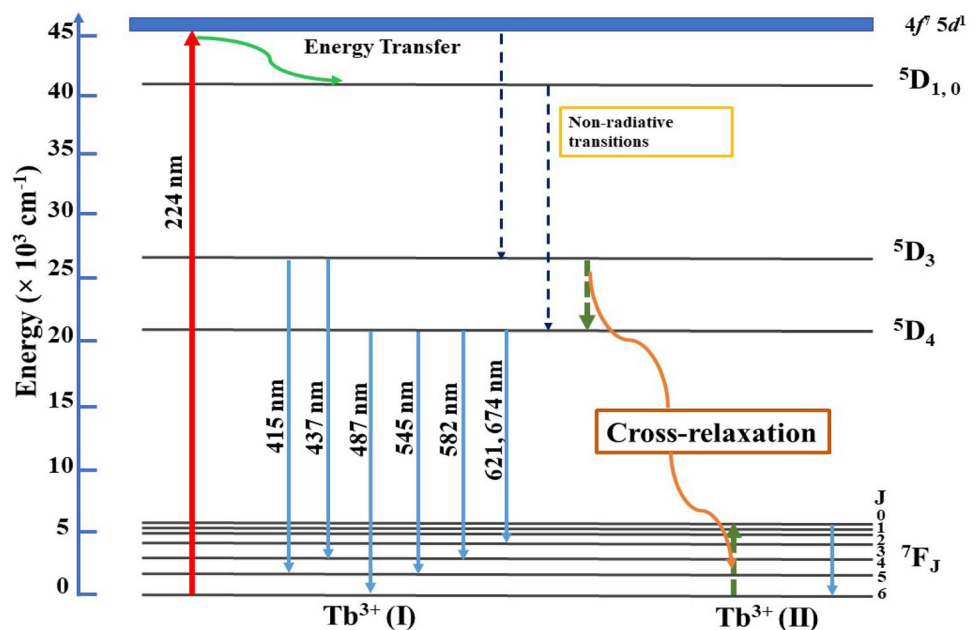**Fig. 8** Normalized Emission spectrum of $Ba_3Gd_{1-x}Tb_xP_3O_{12}$ ($x=0.02$–0.07) nanophosphor scrutinized at $\lambda_{ex}=224$ nm (Color figure online)

energy gap between the excited energy states $^5D_3$–$^5D_4$ and ground state $^7F_6$–$^7F_0$ levels elucidates the cross-relaxation via resonant energy transfer as shown in schematic energy diagram (Fig. 9) [33].

Generally, the transfer of the resonant energies between the two adjacent Tb^{3+} ions can occur via three mechanisms i.e., exchange interaction, electric multipolar interaction and radiation re-absorption. Out of these three possibilities, radiation re-absorption can be discarded as there is no spectral overlapping of excitation and emission bands. Therefore, it is necessary to figure out the critical distance (R_c) to assess the potential mechanism for energy transfer. So, for the $^5D_4$ emission in the $Ba_3Gd_{0.93}Tb_{0.07}P_3O_{12}$ (critical concentration) nanophosphor R_c can be evaluated by using the equation reported by Blasse and Grabmaier and expressed as [34, 35]:

$$R_c = 2\left[\frac{3V}{4\prod x_c N}\right]^{1/3} \tag{6}$$

where V is the volume of the unit cell ($Å^3$), N is the number of replaceable cations in the unit cell and x_c is the critical concentration. After putting $N=4$, $x_c=0.07$ and $V=1148.95\ Å^3$ for the R_c is measured to be 19.87 Å; suggesting that the resonant energy transfer occurs via multipolar interaction among the adjacent trivalent terbium ions in this case. Furthermore, dominating electric multipolar interactions are categorized as dipole–dipole (d–d), dipole–quadrupole (d–q) and quadrupole–quadrupole (q–q) interactions. So, the relationship between the dopant ions concentrations (x) and luminescence intensity (I) can be expressed as [36, 37]:

$$log(I/x) = -\frac{Q}{3}logx + A \tag{7}$$

where A is a constant, x is the concentration of activator ion greater than the critical concentration, Q denotes the

Fig. 9 Energy transfer mechanism for Tb^{3+} ions in $Ba_3Gd_{1-x}Tb_xP_3O_{12}$ ($x=0.02$–0.08) nanophosphor

type of multipolar interaction value of which varies as 6, 8 or 10 for dipole–dipole (d–d), dipole-quadrupole (d-q) and quadrupole–quadrupole (q–q) interactions, respectively. As the graph demonstrated in Fig. 10 shows the relationship between $\log(I/x)$ and $\log(x)$ with the slope value -2.2568 ± 0.11516 results in the value of $Q \approx 6$; indicating that the dipole–dipole interactions are the main cause for the cross-relaxation energy transfer in Tb^{3+} doped $Ba_3GdP_3O_{12}$ nanophosphors.

Also, the decay behavior of $^5D_4$ state in $Ba_3GdP_3O_{12}$:Tb^{3+}, at $\lambda_{ex} = 224$ nm and $\lambda_{em} = 545$ nm, was evaluated. The obtained curves for all $Ba_3Gd_{1-x}Tb_xP_3O_{12}$ nanophosphors are well fitted by the first exponential decay by utilizing the equation [38]:

$$I = I_0 \exp(-t/\tau) \tag{8}$$

where I and I_o are the luminescence intensity at time t and 0 respectively, τ is the fluorescence lifetime and A is a constant. The values of photoluminescent lifetime for different Tb^{3+}-doped samples reveal that the value of τ declines with the increase in the activated concentration (Table 5). Figure 11 represents the single exponential decay of the $Ba_3Gd_{0.93}Tb_{0.07}P_3O_{12}$ which can be viewed in terms of homogenous dispersal of all terbium ions in the host matrix with similar local environment returning at the same rate.

The Commission Internationale de I'Eclairage (CIE) chromaticity coordinates depicts the emission color of the nanophosphors. Figure 12 shows the calculated chromaticity coordinates (x, y) of the $Ba_3Gd_{1-x}P_3O_{12}$: xTb^{3+} ($x = 0.02$, 0.03, 0.04, 0.05, 0.06, 0.07, 0.08) on the CIE 1931 color space chromaticity diagram obtained from emission spectra under the excitation of 224 nm wavelength and charted in Table 5. The chromaticity coordinates for all the synthesized nanophosphors clearly show the tunability from blue
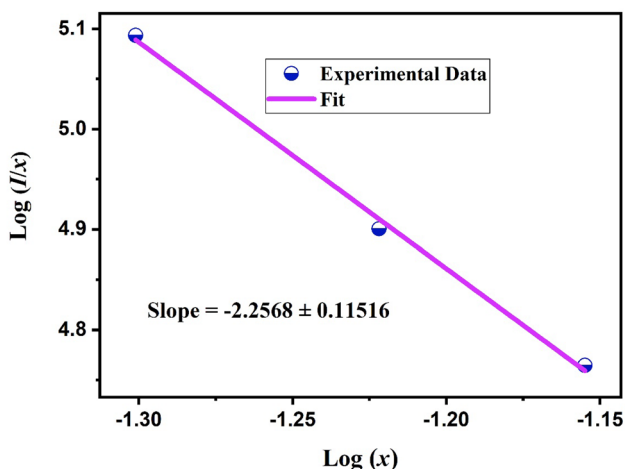
Table 5 CIE1931 chromaticity index and life-time for $Ba_3Gd_xTb_{(1-x)}P_3O_{12}$ (2–8 mol %) nanophosphors

Tb^{3+} concentrations (mol%)	Color coordinates (x, y)	Life time (ms)
2	(0.1739, 0.2166)	3.91268
3	(0.1795, 0.2498)	3.77643
4	(0.1815, 0.2656)	3.58031
5	(0.1875, 0.2943)	3.52
6	(0.2022, 0.3024)	3.46827
7	(0.20, 0.34)	3.43911
8	(0.2145, 0.3350)	3.43281

to green region on the intensification of Tb^{3+} ions in the host lattice. The luminescent tunability in $Ba_3GdP_3O_{12}$: Tb^{3+} (2–8 mol%) finds its use in the wider range of display devices or in solid state lighting.

4 Conclusion

A series of blue–green $Ba_3Gd_{(1-x)}P_3O_{12}$: xTb^{3+} nanocrystals has been efficaciously synthesized via urea-assisted solution-combustion technique. Its structural morphology, energy-transfer mechanism, photoluminescent (PL) excitation-emission and decay time behavior were examined in detail by means of powder X-ray Diffraction (XRD), Transmission Electron Microscopy (TEM), Diffuse Reflectance (DR) and PL spectroscopy. The Rietveld investigation shows the cubic phase formation of all the nanophosphors with I-43d (220) space group and concludes that Gd^{3+} ions can be well replaced by Tb^{3+} ions without any major modification in the crystal structure
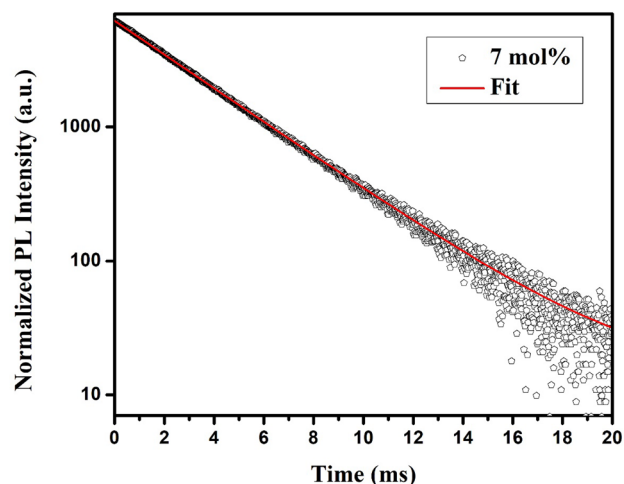

Fig. 10 Plot of log (I/x) as a function of log(x) in $Ba_3Gd_{1-x}Tb_xP_3O_{12}$ nanophosphors

Fig. 11 The luminescence decay curve for 545 nm ($^5D_4 \rightarrow {}^7F_5$ of Tb^{3+}) emission of $Ba_3Gd_{0.93}Tb_{0.07}P_3O_{12}$ nanophosphors
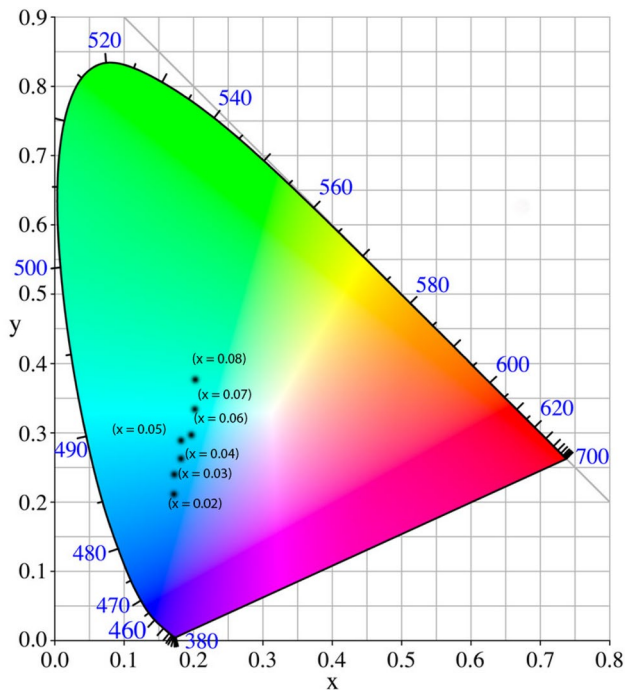
Fig. 12 CIE chromaticity diagram for $Ba_3Gd_{1-x}Tb_xP_3O_{12}$ ($x = 0.02$–0.08) nanophosphors

of the host matrix. The optical band-gap of the host was assessed to be 4.9 eV, offering high potential as a host for lanthanide activators. Upon excitation at $\lambda_{ex} = 224$ nm, the photoluminescent emission spectra showed the two main characteristic peaks at 545 nm and 478 nm as a result of $^5D_4 \rightarrow ^7F_5$ (green and magnetic-dipole) and $^5D_4 \rightarrow ^7F_6$ (blue and electric-dipole) transitions, respectively. The decay analysis exhibited that the activator resides in a single crystallographic site, a fact that is also supported by the Rietveld refinement. The R_c of the energy transfer (19.87 Å) combined with Dexter's modeling provides information about energy migration via dipole–dipole interactions. The PL result displayed that the blue-to-green tunable emission can be attained simply via varying the activator concentration, with 7 mol% as the optimal concentration for standard CIE coordinates of green emission. All the results propose that $Ba_3Gd_{(1-x)}P_3O_{12}$: xTb^{3+} crystals can find their usage as a green phosphor component in display gadgets and solid-state lighting.

References

1. D. Kima, B.K. Moona, S.H. Parka, J.H. Kima, J.H. Jeonga, Full-color tuning in europium doped phosphosilicate phosphors via adjusting crystal field modulation or excitation wavelength. J. Alloys Compd. **770**, 411–418 (2019)
2. T.M. Katona, P.M. Pattison, S. Paolini, Status of solidstate lighting product development and future trends for general illumination. Rev. Cell. Biol. **7**, 263–281 (2016)
3. H. Zhu, C.C. Lin, W. Luo, S. Shu, Z. Liu, Y. Liu, J. Kong, E. Ma, Y. Cao, R. Liu, X. Chen, Highly efficient non-rare-earth red emitting phosphor for warm white light-emitting diodes. Nat. Commun. **5**, 4312 (2014)
4. N. Salah, S.S. Habib, Z.H. Khan, Quantum effect on the energy levels of Eu^{2+}doped K$_2$Ca$_2$(SO$_4$)$_3$ nanoparticles. J. Fluoresc. **20**, 1009–1015 (2010)
5. L.M. Becerra, R.V. Arreguin, U. Balderas, S.C. Tellez, H.M. Sanchez, C. Falcony, Luminescent characteristics of layered yttrium oxide nano-phosphors doped with europium. J. Appl. Phys. **121**, 125111 (2017)
6. C. Manjunatha, M.S. Rudreshaa, R.H. Krishnab, B.M. Nagabhushanab, B.M. Walshc, K.R. Nagabhushanad, B.S. Panigrahi, Spectroscopic studies of strong red emitting Sr$_2$SiO$_4$:Eu^{3+} nanophosphors with high color purity for application in WLED using Judd-Ofelt theory and TL glow curve analysis. Opt. Mater. **85**, 363–372 (2018)
7. E. Pavitra, G.S.R. Raju, J.H. Oh, L.K. Bharath, J.H. Jeong, Y.S. Huh, J.S. Yu, (BaSr)$_2$SiO$_4$:Eu^{2+} nanorods with enhanced luminescence properties as green-emitting phosphors for white LED applications. Dyes Pigments **142**, 447–456 (2017)
8. M. Jiao, N. Guo, W. Lü, Y. Jia, W. Lv, Q. Zhao, B. Shaoa, H. You, Synthesis, structure and photoluminescence properties of europium-, terbium-, and thulium-doped Ca$_3$Bi(PO$_4$)$_3$ phosphors. Dalton Trans. **42**, 12395 (2013)
9. Z. Fua, L. Maa, S. Sahia, R. Halla, W. Chen, Influence of doping concentration on valence states of europium in SrAl2O4: Eu phosphors. J. Lumin. **143**, 657–662 (2013)
10. V. Singha, S. Watanabeb, T.K.G. Rao, H.Y. Kwak, Luminescence and defect centres in Tb^{3+} doped LaMgAl$_{11}$O$_{19}$ phosphors. Solid State Sci. **12**, 1981–1987 (2010)
11. G.H. Dieke, *Spectra and Energy Levels of Rare Earth Ions in Crystals* (Inter-science Publishers, Olney, 1968), p. 253
12. B. Ramesh, G.R. Dillip, B. Rambabu, S.W. Joo, B.D. Raju, Structural studies of a green-emitting terbium doped calcium zinc phosphate phosphor. J. Mol. Struct. **1155**, 568–572 (2018)
13. V.R. Panse, N.S. Kokode, S.J. Dhoble, Tb^{3+} doped Sr$_2$(BO$_3$)Cl green emitting phosphor for solid state lighting. Adv. Mater. Lett. **5**, 604–610 (2014)
14. A.G.B. Jr, S.A.M. Lima, A.M. Pires, Energy transfer between terbium and europium ions in barium orthosilicate phosphors obtained from sol-gel route. J. Lumin. **199**, 372–378 (2018)
15. N. Guo, W. Lu, Y. Jia, W. Lv, Q. Zhao, H. You, Eu^{2+} & Mn^{2+}-coactivated Ba$_3$Gd(PO$_4$)$_3$ orange-yellow emitting phosphor with tunable color tone for UV-excited white LEDs. Chem. Phys. Chem. **14**, 192–197 (2013)
16. Q. Di, Q. Xu, L. Han, J. Sun, Synthesis and luminescence properties of Eu^{3+}-doped Ba$_3$Gd(PO$_4$)$_3$ phosphors for light-emitting diodes. Opt. Eng. **54**, 035104 (2015)
17. S. Ekambaram, K.C. Patil, J. Alloys Compd. **448**, 7 (1997)
18. N.N. Greenwood, A. Earnshaw, *Chemistry of the Elements* (Elsevier, Amsterdam, 1997), pp. 1230–1242
19. H. Dahiya, M. Dalal, A. Siwach, M. Dahiya, D. Kumar, Cool white light emitting Ba$_5$Zn$_4$Y$_8$O$_{21}$:Dy^{3+} nanophosphors for single phased WLEDs. J. Mater. Sci. **29**, 20750–20758 (2018)

20. M. Dalal, V.B. Taxak, J. Dalal, A. Khatkar, S. Chahar, R. Devi, S.P. Khatkar, Crystal structure and Judd-Ofelt properties of a novel color tunable blue-white-red $Ba_5Zn_4Y_8O_{21}$:Eu^{3+} nanophosphor for near-ultraviolet based WLEDs. J. Alloys Compd. **698**, 662–672 (2017)

21. D.S. Kshatri, A. Khare, Characterization and optical properties of Dy^{3+} doped nanocrystalline $SrAl_2O_4$: Eu^{2+} phosphor. J. Alloys Compd. **588**, 488–495 (2014)

22. A. Chowdhury, B. Biswas, M. Majumder, M.K. Sanyal, B. Mallik, Studies on phase transformation and molecular orientation in nanostructured zinc phthalocyanine thin films annealed at different temperatures. Thin Solid Films **520**, 6695–6704 (2012)

23. J. Qiao, Z. Xia, Z. Zhang, B. Hu, Q. Liu, Near UV-pumped yellow-emitting $Sr_9MgLi(PO_4)_7$:Eu^{2+} phosphor for white-light LEDs. Sci. China Mater. **61**, 985–992 (2018)

24. S. Devi, A. Khatkar, V.B. Taxak, M. Dalal, S. Chahar, J. Dalal, S.P. Khatkar, Optical properties of trivalent samarium-doped $Ba_5Zn_4Y_8O_{21}$ nano-diametric rods excitable by NUV light. J. Alloys Compd. **767**, 409–418 (2018)

25. K. Thomas, D. Alexander, S. Sisira, P.R. Biju, N.V. Unnikrishnan, M.A. Ittyachen, C. Joseph, NUV/blue LED excitable intense green emitting terbium doped lanthanum molybdate nanophosphors for white LED applications. J. Mater. Sci. **28**, 17702–17709 (2017)

26. X. Gaoa, C. Lia, S. Lib, H. Zhanga, Z. Lia, Y. Honga, J. Sun, Intense green/blue light emission of Zn_2GeO_4 nanophosphors doped Tb^{3+} ions under 265-nm excitation. J. Lumin. **190**, 457–461 (2017)

27. D. Kumar, M. Sharma, D. Haranath, O.P. Pandey, Facile route to produce spherical and highly luminescent Tb^{3+} doped Y_2O_3 nanophosphors. J. Alloys Compd. **695**, 726–736 (2017)

28. S.J. Motloung, S.K.K. Shaat, K.G. Tshabalalaa, O.M. Ntwaeaborwa, Structure and photoluminescent properties of green-emitting terbium-doped $GdV_{1-x}P_xO_4$ phosphor prepared by solution combustion method. Luminescence **31**, 1069–1076 (2016)

29. X. Yang, B. Zhang, T. Xu, L. Wang, J. Shen, Q. Zhang, Enhanced luminescent intensity of Sr_2SiO_4:Tb^{3+} phosphors by charge compensation (Li^+) addition. J. Mater. Sci. **27**, 9448–9453 (2016)

30. B. Li, X. Huang, H. Guo, Y. Zeng, Energy transfer and tunable photoluminescence of LaBWO6:Tb3 +, Eu3 + phosphors for near-UV white LEDs. Dyes Pigments **150**, 67–72 (2018)

31. X. Huang, B. Li, H. Guo, Synthesis, photoluminescence, cathodoluminescence, and thermal properties of novel Tb^{3+}-doped BiOCl green-emitting phosphors. J. Alloys Compd. **695**, 2773–2780 (2017)

32. L. Wang, L. Shi, N. Liao, H. Jia, P. Du, Z. Xi, L. Wang, D. Jin, Photoluminescence properties of Y_2O_3:Tb^{3+} and YBO_3:Tb^{3+} green phosphors synthesized by hydrothermal method. Mater. Chem. Phys. **119**, 490 (2010)

33. X. Zhou, S. Jiang, G. Xiang, X. Tang, X. Luo, L. Li, X. Zhou, Tunable emission color of Li_2SrSiO_4:Tb^{3+} due to cross-relaxation process and optical thermometry investigation. J. Am. Ceram. Soc. **101**, 3076–3085 (2018)

34. G. Blasse, Energy transfer in oxidic phosphors. Phys. Lett. **28**, 444–445 (1968)

35. G. Ramakrishnaa, H. Nagabhushana, R.B. Basavaraj, S.C. Prashantha, S.C. Sharma, R. Naik, K.S. Anantharaju, Green synthesis, structural characterization and photoluminescence properties of Sm^{3+} co-doped Y_2SiO_5:Ce^{3+} nanophosphors for wLEDs. Optik **127**, 5310–5315 (2016)

36. D. Dexter, J. Schulman, Theory of concentration quenching in inorganic phosphors. J. Chem. Phys. **22**, 1063–1070 (1954)

37. Y. Fang, X. Huang, Y. Juang, S. Chu, Color-tunable blue to green $Ca_{4-1.5x}Ta_2O_9$: xTb^{3+} phosphor: cross relaxation mechanism and thermal stability. J. Am. Ceram. Soc. **95**, 1613–1618 (2012)

38. A. Prasad, A.S. Rao, M. Gupta, G.V. Prakash, Morphological and luminescence studies on $KGdF_4$:Yb^{3+}/Tb^{3+} up-conversion nanophosphors. Mater. Chem. Phys. **219**, 13–21 (2018)